A Hessian Recovery Based Linear Finite Element Method for Molecular Beam Epitaxy Growth Model with Slope Selection

Minqiang Xu[1,2] and Qingsong Zou[3,*]

[1] *College of Science, Zhejiang University of Technology, Hangzhou, Zhejiang 310023, China*

[2] *School of Computer Science and Engineering, Sun Yat-Sen University, Guangzhou, Guangdong 510275, China*

[3] *School of Computer Science and Engineering, and Guangdong Province Key Laboratory of Computational Science, Sun Yat-Sen University, Guangzhou, Guangdong 510275, China*

Abstract. In this paper, we present a Hessian recovery based linear finite element method to simulate the molecular beam epitaxy growth model with slope selection. For the time discretization, we apply a first-order convex splitting method and second-order Crank-Nicolson scheme. For the space discretization, we utilize the Hessian recovery operator to approximate second-order derivatives of a C^0 linear finite element function and hence the weak formulation of the fourth-order differential operator can be discretized in the linear finite element space. The energy-decay property of our proposed fully discrete schemes is rigorously proved. The robustness and the optimal-order convergence of the proposed algorithm are numerically verified. In a large spatial domain for a long period, we simulate coarsening dynamics, where 1/3-power-law is observed.

1 Introduction

In recent years, the molecular beam epitaxy (MBE) growth approach has become a powerful tool for thin-film deposition of single crystal [15,43]. So MBE growth technique has been widely applied in material science, especially in semi-conductor manufacture and

---

*Corresponding author.

Emails: mqxu@zjut.edu.cn (M. Xu), mcszqs@mail.sysu.edu.cn (Q. Zou)

nano-technology industry. In previous works, there are mainly three types of mathematical modelings to study dynamics of the MBE growth process: atomistic models [2,19], continuum models [23,31,42] and hybrid models [6,14].

We are interested in the continuum model with slope selection introduced by Moldovan and Golubovic [29]. It describes the evolution of the MBE growth with isotropic symmetry current, of which the governing equation takes the form [22]:

$$\begin{cases} \partial_t u = -\varepsilon \Delta^2 u + \nabla \cdot (|\nabla u|^2 \nabla u - \nabla u) & \text{in } \Omega \times [0,T], \\ u(\cdot,0) = u_0(\cdot) & \text{in } \Omega, \end{cases} \tag{1.1}$$

where Ω is a smooth domain, ε is a positive constant, and the unknown function u represents the epitaxy surface height of the thin film. Moreover, we suppose u satisfies a certain periodic boundary condition or Neumann boundary conditions $\partial_{\mathbf{n}} u|_{\partial \Omega} = 0$ and $\partial_{\mathbf{n}} \Delta u|_{\partial \Omega} = 0$, where $\mathbf{n}$ is the outward normal on the boundary. The MBE equation (1.1) can be derived via an L^2-gradient flow of the effective free energy functional [11,20]

$$E(u) := \int_{\Omega} \left(\frac{\varepsilon}{2} |\Delta u|^2 + \frac{1}{4} (|\nabla u|^2 - 1)^2 \right) d\Omega, \tag{1.2}$$

of which the first term represents the surface diffusion effect [11] and the second term describes the Ehrlich-Schwoebel effect [22]. Thanks to the flux free condition at the boundary, it is trivial to show that the energy decay property

$$\frac{dE(u)}{dt} = -\|u_t\|_0^2 \le 0, \quad \forall t > 0,$$

and the total mass conservation property

$$\frac{d}{dt} \int_{\Omega} u \, d\Omega = 0,$$

always hold for the solution of the MBE equation (1.1).

During the past several decades, the numerical solution for (1.1) (see e.g., [4,6,8–10, 12–14,18,21,24,25,27,28,32–35,37,38,41,44,47,48,51]) has been intensively investigated based on variants of temporal discretization and spatial discretization techniques.

On temporal-discretization, two popular approaches can guarantee the energy decay property of the numerical solution. The basic idea of the first approach is so-called *convex splitting* which splits the nonlinear term to the convex part which will be treated implicitly and the concave part which will be treated explicitly, see [5,41,44,47]. The unconditional energy decay property and the unique solvability of the numerical solution of this approach could be easily derived. However, such methods lead to a nonlinear algebraic system that requires high computational cost. The second approach is the so-called *linear stabilization approach* which treats the nonlinear term only explicitly and guarantees the energy stability by adding a linear artificial penalty term, see [38–40,49]. Such a method

is linear and simple to implement. However, no theory guarantees the corresponding energy decay property. Recently, there have been some new developments regarding this method, for example, Qiao et al. in [35] proposed a second-order Crank–Nicolson time-stepping scheme without adding artificial terms and a corresponding adaptive time step strategy based on the energy variation for the MBE model (1.1), making the phase field simulation more efficient, Li et al. in [24] removed the Lipschitz assumption on the nonlinearity and proved unconditional energy decay for the stabilized time-stepping methods.

More recently, two novel approaches known as IEQ and SAV are developed to solve the phase field models. Both of these algorithms use the energy quadratization approach to convert the primitive system into a new equivalent system. The modified energy is proven to be unconditionally stable. Yang et al. in [48] and Chen et al. in [9] proposed second-order Crank–Nicolson and Adam–Bashforth time-stepping schemes based on IEQ for MBE model (1.1). By using the SAV technique, Ji et al. in [18] designed an adaptive second-order Crank–Nicolson time-stepping scheme for the time-fractional molecular beam epitaxial models. There are also some other energy decay preserving numerical algorithms, for example, Chen et al. in [8] presented a new multi-step Crank–Nicolson, which is proved to possess properties of total mass conservation and unconditionally energy stability. Lu et al. in [27] developed a second- and third- order fully discrete scheme for (1.1) based on the local structure-preserving algorithm. Cheng and Wang in [7] gave a error estimate of second order accurate SAV numerical method for the epitaxial thin film equation.

As for spatial discretization of MBE model (1.1) with periodic boundary condition, classic numerical methods including finite difference methods [33, 41, 44, 48], spectral methods [8, 24, 25], and finite element methods [4, 32] have been studied. In [33], Zhang et al. applied a finite difference scheme for solving the MBE model (1.1), and the stability and optimal convergence order of the proposed method were discussed. In [32], Qiao et al. established the error estimation of the mixed element method for (1.1). For the MBE model (1.1) with the Neumann boundary condition, Xia [45] developed a fully discrete stable discontinuous Galerkin method, and Lu et al. in [27] proposed a finite difference scheme.

We focus on finite element methods for the MBE equation (1.1). Recently, a nonconforming finite element method called gradient recovery based linear finite element method (GRBL–FEM) has been presented to solve high order differential equations in [3, 17, 26]. The key idea of the GRBL–FEM is using gradient recovery operators [50, 52, 53] "lift" discontinuous piecewise constant function to a continuous piecewise linear function, and hence second-order differentiation derivatives are possible. The GRBL–FEM uses the least degree of freedom, therefore it is simple and straightforward to implement.

In our previous work [46], we developed a Hessian recovery based linear finite element method (HRBL–FEM) for solving the Cahn–Hilliard (C–H) equation. The main purpose of this work is to design some HRBL–FEMs combining convex splitting methods presented in [5, 47] to solve the MBE equation (1.1) with periodic boundary condi-

tions or Neumann boundary conditions. We prove that the fully discrete scheme of the MBE equation with periodic boundary condition preserves the energy decay and mass conservation properties. Comparing to other existing numerical methods for spatial discretization of the MBE model, our HRBL–FEMs enjoy some advantages. First, linear elements induce smaller degrees of freedom in comparison to C^1 or mixed elements, which hence leads to easier implementation and less computational cost. Second, the recovery operators can be defined on a general unstructured grid, and our algorithms thus work naturally for arbitrary geometries in comparison with regular domains used by finite difference methods or spectral methods. Although our schemes are simple and straightforward, they have very nice convergence properties. The optimal-order convergence under L^2- and H^1- error norm are numerically observed both on a square domain and a circular domain. We also discover that there is a phenomenon of superconvergence between the recovered Hessian and the exact one. By utilizing the adaptive time-stepping algorithm proposed in [35], we simulate the MBE equation on a large area during a long period, where the height grows like $\mathcal{O}(t^{1/3})$ and the energy decays like $\mathcal{O}(t^{-1/3})$ are observed.

The rest of the paper is organized as follows: In Section 2, some notations and a variational formulation of the (1.1) are given. In Section 3, we first introduce the recovery technique based on a least-square fitting; then, we apply the recovery based finite element method to discrete the MBE equation (1.1). Energy decay and mass conservation properties of the fully discrete scheme are discussed as well. In Section 4, we numerically demonstrate the accuracy of the proposed scheme and simulate the coarsening dynamics through some benchmark examples. Finally, we end the paper with a brief conclusion in Section 5.

2 The variational formulations of the MBE model (1.1)

We shall use the standard notation for Sobolev spaces H^i and their associated norms $\|\cdot\|_i$ and seminorms $|\cdot|_i$ (see, e.g., [1]). In particular, $(\cdot,\cdot)$ is the L^2-inner product. Let

$$H_{\mathrm{per}}^i(\Omega) = \{u | u \in H^i(\Omega) \text{ with periodic boundary condition}\}, \quad i = 1, 2,$$

and

$$L^2(0,T;X) = \left\{ v : (0,T) \to X, \ \|v\|_{L^2(0,T;X)} = \left(\int_0^T \|v\|_X^2 dt \right)^{\frac{1}{2}} < \infty \right\}.$$

For the periodic boundary conditions, the variational formulation of the MBE equation is to find $u \in L^2(0,T;H_{\mathrm{per}}^2)$ such that

$$\left(\frac{\partial u}{\partial t}, v \right) + \epsilon(\Delta u, \Delta v) + ((|\nabla u|^2 - 1)\nabla u, \nabla v) = 0, \quad \forall v \in H_{\mathrm{per}}^2. \tag{2.1}$$

To deal the Neumann boundary conditions $\partial_\mathbf{n} u = \partial_\mathbf{n} \Delta u = 0$, we apply Nitsche's technique [30] to impose the Neumann boundary condition $\partial_\mathbf{n} u = 0$ weakly on the variational

formulation. We introduce a bilinear form

$$a(w,v) = \int_\Omega \Delta w \Delta v \, dz - \int_{\partial\Omega} \Delta w \partial_\mathbf{n} v \, ds - \int_{\partial\Omega} \partial_\mathbf{n} w \Delta v \, ds$$

$$+ \gamma \int_{\partial\Omega} \partial_\mathbf{n} w \partial_\mathbf{n} v \, ds, \quad \forall v, w \in H^2(\Omega), \tag{2.2}$$

with γ is a positive stability parameter.

Now we claim that the weak solution of (1.1) is a function $u \in H^2(\Omega)$ that satisfies the variational equation

$$\left(\frac{\partial u}{\partial t}, v\right) + \varepsilon a(u,v) + (|\nabla u|^2 - 1)\nabla u, \nabla v) = 0, \quad \forall v \in H^2(\Omega). \tag{2.3}$$

In fact, on one hand, we get immediately that u satisfies (2.3) provided that $u \in H^2(\Omega)$ is the solution of (1.1). On the other hand, if $u \in C^4(\Omega)$ and $u_t \in C(\Omega)$ satisfying (2.3), then by applying the basic technology of integration by parts, we have

$$\left(\frac{\partial u}{\partial t} + \varepsilon \Delta^2 u - \nabla \cdot (|\nabla u|^2 - 1)\nabla u), v\right) - \varepsilon \int_{\partial\Omega} \partial_\mathbf{n} u \Delta v \, ds$$

$$+ \varepsilon\gamma \int_{\partial\Omega} \partial_\mathbf{n} u \partial_\mathbf{n} v + \int_{\partial\Omega} (-\varepsilon\nabla\Delta u + (|\nabla u|^2 - 1)\nabla u) \cdot \mathbf{n} v \, ds = 0. \tag{2.4}$$

Choosing $v \in C_0^\infty(\Omega)$ in (2.4), we deduce that

$$\frac{\partial u}{\partial t} + \varepsilon \Delta^2 u - \nabla \cdot (|\nabla u|^2 - 1)\nabla u = 0.$$

As a consequence, the Eq. (2.4) becomes

$$-\varepsilon \int_{\partial\Omega} \partial_\mathbf{n} u \Delta v \, ds + \varepsilon\gamma \int_{\partial\Omega} \partial_\mathbf{n} u \partial_\mathbf{n} v + \int_{\partial\Omega} (\varepsilon\partial_\mathbf{n}\Delta u + (|\nabla u|^2 - 1)\partial_\mathbf{n} u) v \, ds = 0, \quad v \in H^2(\Omega).$$

Due to the arbitrariness of $v \in H^2(\Omega)$ in the above equation, we obtain that

$$\partial_\mathbf{n} u = \partial_\mathbf{n} \Delta u = 0,$$

which implies that u is the strong solution of (1.1). Therefore, the weak formulation (2.3) is a variational formulation of (1.1).

Remark 2.1. When using the penalty method or Lagrange multiplier method, one usually deals the Neumman boundary condition $\partial_\mathbf{n} u = 0$ by imposing it into the solution space directly. Correspondingly, one also requires the function in the approximate space "strongly" satisfy this Neumann boundary condition. Here, using the Nitsche's technique, the Neuwmann boundary condition is "weakly" imposed in the variational formulation, so that the standard linear finite element space can be chosen as our discrete solution space.

3   A recovery based linear finite element method

In this section, we design a recovery-technique-based finite element method for the MBE equation (1.1). We first give the recovery technique. Next, we explain how to discretize (1.1) in a linear finite element space.

3.1   A Hessian recovery operator in linear finite element spaces

Let $\mathcal{T}_h$ be a triangulation of the domain Ω with mesh-size h. We use $\mathcal{N}_h$ and $\mathcal{E}_h$ to denote the set of vertices and edges of $\mathcal{T}_h$. We denote by V_h the standard $\mathcal{P}_1$ finite element space according to $\mathcal{T}_h$

$$V_h := \{v_h \in H^1(\Omega),\, v_h|_K \in \mathcal{P}_1,\, \forall K \in \mathcal{T}_h\},$$

and

$$V_h^{\mathrm{per}} := \{v_h \in H_{\mathrm{per}}^1(\Omega),\, v_h|_K \in \mathcal{P}_1,\, \forall K \in \mathcal{T}_h\}.$$

As known to all, the gradient of a function $v_h \in V_h$ is not well-defined on an edge $E \in \mathcal{E}_h$ and the second order derivative of a function $v_h \in V_h$ equals to 0 in each element $T \in \mathcal{T}_h$. Denote $V_h^4 = \{(v_{i,j})_{2\times 2} | v_{i,j} \in V_h,\, i,j=1,2\}$. In the following, we propose the quadratic fitting method to calculate the approximate second order derivatives of v_h. In other words, we will define a Hessian recovery operator H_h from V_h to V_h^4 which maps a function $v_h \in V_h$ to $H_h v_h \in V_h^4$ so that $H_h v_h$ can be regarded as an approximation of the Hessian matrix of v_h in some sense.

Obviously, $H_h v_h$ is completely determined by nodal values, consequently, it is sufficient to define the value $(H_h v_h)(z)$ for all $z \in \mathcal{N}_h$. For this purpose, we first construct a local patch $\mathcal{L}_z$ associated with z. Given a vertex $z \in \mathcal{N}_h$, the local patch $\mathcal{L}_z$ is a polygon surrounding the node z. It is constructed by the following strategy. The patch $\mathcal{L}_z$ is first composed of the elements ring surrounding the vertex z. To this ring of elements, enrich another ring which is consisted of element neighbors (sharing at least a vertex) of the first ring. Repeat the procedure until the patch contains at least six vertices. Over that patch $\mathcal{L}_z$, the sampling points are all vertices adjacent to elements of the patch $\mathcal{L}_z$.

Using the sampling points in $\mathcal{L}_z$, we fit a quadratic polynomial p_z at the vertex z in the following least-squares sense

$$p_z = \arg\min_{p\in\mathbb{P}^2(\mathcal{L}_z)} \sum_{x\in\overline{\mathcal{L}}_z\cap\mathcal{N}_h} |p(x) - v_h(x)|^2.$$

Then, the value of recovered Hessian at the node z is defined by

$$(H_h v_h)(z) = \begin{pmatrix} H_h^{xx} v_h(z) & H_h^{xy} v_h(z) \\ H_h^{yx} v_h(z) & H_h^{yy} v_h(z) \end{pmatrix} = \begin{pmatrix} \dfrac{\partial^2 p_z}{\partial x^2}(z) & \dfrac{\partial^2 p_z}{\partial x\partial y}(z) \\ \dfrac{\partial^2 p_z}{\partial y\partial x}(z) & \dfrac{\partial^2 p_z}{\partial y^2}(z) \end{pmatrix}. \tag{3.1}$$

By linear interpolation of nodal values, we have

$$H_h v_h = \sum_{z \in \mathcal{N}_h} H_h v_h(z) \phi_z \in V_h^4.$$

Clearly, the Hessian matrix function $H_h v_h$ satisfies the symmetric property $H_h^{xy} = H_h^{yx}$. Based on H_h, we define a recovery Laplacian operator $\Delta_h : V_h \to V_h$ as

$$\Delta_h v_h = H_h^{xx} v_h + H_h^{yy} v_h. \tag{3.2}$$

Note that in the same way, we can recover the gradient of v_h by letting

$$(G_h v_h)(z) = \nabla p_z(z), \quad \forall z \in \mathcal{N}_h, \tag{3.3}$$

and

$$G_h v_h = (G_h^x v_h, G_h^y v_h) = \sum_{z \in \mathcal{N}_h} G_h v_h(z) \phi_z \in V_h^2.$$

Remark 3.1. On regular pattern uniform meshes, the recovery Laplacian operator Δ_h is the well-known five-point-finite-difference stencil of the Laplace operator, see [16,46] for the details.

3.2 Time discretization for problem (1.1)

In this section, we utilize a first-order convex splitting scheme and a second-order Crank-Nicolson (CN) scheme to carry out the time discretization. The application of these two presented schemes to discrete MBE-type equations can be found in [5,47]. Let the time step size be $\Delta t = \frac{T}{N}$, $u^0(x) = u(x,0)$, and $u^n(x) \approx u(x,t_n)$ with $t_n = n\Delta t$, $n = 1, 2, \cdots, N$.

The first-order convex splitting scheme for the MBE model (1.1) is of the form

$$\frac{u^{n+1} - u^n}{\Delta t} = -\varepsilon \Delta^2 u^{n+1} + \nabla \cdot (|\nabla u^{n+1}|^2 \nabla u^{n+1} - \nabla u^n), \tag{3.4}$$

and the second-order CN scheme for the MBE model (1.1) reads as:

$$\frac{u^{n+1} - u^n}{\Delta t} = -\varepsilon \frac{\Delta^2 (u^{n+1} + u^n)}{2} + \nabla \cdot \frac{|\nabla u^{n+1}|^2 + |\nabla u^n|^2}{2} \frac{\nabla u^{n+1} + \nabla u^n}{2} - \frac{\Delta u^{n+1} + \Delta u^n}{2}. \tag{3.5}$$

3.3 Fully discrete schemes for problem (1.1) with periodic boundary conditions

In this subsection, we present and discuss two schemes for problem (1.1) with periodic boundary conditions by using (3.4), (3.5), and (2.1).

The combination of (3.4) and Hessian recovery based linear element method lead to the following fully discretized scheme for (1.1).

Scheme 1: The Hessian recovery based linear element scheme with respect to Eq. (2.1) reads as: finding $\{u_h^n\}_{n\geq 1}\in V_h^{\text{per}}$ such that for $n=0,1,\cdots,N$,

$$\frac{1}{\Delta t}(u_h^{n+1},v_h)+\varepsilon(\Delta_h u_h^{n+1},\Delta_h v_h)+(|\nabla u_h^{n+1}|^2\nabla u_h^{n+1},\nabla v_h)$$
$$=\frac{1}{\Delta t}(u_h^n,v_h)+(\nabla u_h^n,\nabla v_h),\forall\, v_h\in V_h^{\text{per}}, \tag{3.6}$$

where $u_h^0=\mathcal{P}_h u_0$ and $\mathcal{P}_n$ is the L^2 projection operator on V_h.

The combination of CN approximation and Hessian recovery based linear element method lead to the following fully discretized scheme for (1.1).

Scheme 2: The Hessian recovery based linear element scheme with respect to (2.1) reads as: finding $\{u_h^n\}_{n\geq 1}\in V_h^{\text{per}}$ such that for $n=0,1\cdots,N$,

$$\frac{1}{\Delta t}\left(u_h^{n+1}-u_h^n,v_h\right)+\epsilon\left(\frac{\Delta_h u_h^{n+1}+\Delta_h u_h^n}{2},\Delta_h v_h\right)$$
$$+\left(\frac{|\nabla u_h^{n+1}|^2+|\nabla u_h^n|^2}{2}\frac{\nabla(u_h^{n+1}+u_h^n)}{2},\nabla v_h\right)-\left(\nabla\frac{u_h^{n+1}+u_h^n}{2},\nabla v_h\right)$$
$$=0,\quad\forall v_h\in V_h^{\text{per}}, \tag{3.7}$$

where $u_h^0=\mathcal{P}_h u_0$ and $\mathcal{P}_n$ is the L^2 projection operator on V_h.

Remark 3.2. Note that both the Schemes 1 and 2 are nonlinear, it is not trivial to show their unique solvability. However, this unique solvability can be proved by the same arguments proposed in [4,33].

In practice, the Schemes 1 and 2 should be calculated by using the Newton's iterative method. Note that in each iteration step of the Newton's method, the coefficient matrix of the resulting linear system is symmetric and positive definite, so the iteration solution in each Newton's iterative step is uniquely determined.

Next we will discuss the mass and energy law of the presented fully discrete schemes (3.6) and (3.7). We will first define discrete mass M^n and energy E^n of numerical solution u_h at t_n as follows:

$$M^n:=(u_h^n,1),\quad E^n:=\frac{\epsilon}{2}\|\Delta_r u_h^n\|_0^2+\frac{1}{4}\||\nabla u_h^n|^2-1\|_0^2.$$

Theorem 3.1. *The fully discrete scheme* (3.6) *is unconditionally energy-stable.*

Proof. Choosing $v_h=u_h^{n+1}-u_h^n$ in Eq. (3.6) leads to

$$\frac{1}{\Delta t}\|u_h^{n+1}-u_h^n\|_0^2+\epsilon\|\Delta_h u_h^{n+1}\|^2-\epsilon(\Delta_h u_h^{n+1},\Delta_h u_h^n)$$
$$+(|\nabla u_h^{n+1}|^2\nabla u_h^{n+1},\nabla u_h^{n+1}-\nabla u_h^n)-(\nabla u_h^n,\nabla(u_h^{n+1}-u_h^n))=0. \tag{3.8}$$

M. Xu and Q. Zou / Adv. Appl. Math. Mech., **16** (2024), pp. 1-23

9

Using the identity $-ab = (a-b)^2/2 - (a^2+b^2)/2$, we have

$$-(\Delta_h u_h^{n+1}, \Delta_h u_h^n) = \frac{\|\Delta_h u_h^{n+1} - \Delta_h u_h^n\|^2}{2} - \frac{\|\Delta_h u_h^{n+1}\|^2 + \|\Delta_h u_h^n\|^2}{2}. \tag{3.9}$$

Denote

$$F_+(u) = \frac{1}{4}|\nabla u|^4 \quad \text{and} \quad F_-(u) = -\frac{1}{2}|\nabla u|^2.$$

By Taylor expansion and the fact that $F_+''(u) \geq 0$ and $F_-''(u) \leq 0$, there exist ξ_1 and ξ_2 such that

$$F_+(u_h^n) - F_+(u_h^{n+1}) = F_+'(u_h^{n+1}) \circ (u_h^n - u_h^{n+1}) + \frac{F_+''(\xi_1)}{2} \circ (u_h^{n+1} - u_h^n)^2$$
$$\geq F_+'(u_h^{n+1}) \circ (u_h^n - u_h^{n+1})$$

and

$$F_-(u_h^{n+1}) - F_-(u_h^n) = F_-'(u_h^n) \circ (u_h^{n+1} - u_h^n) + \frac{F_-''(\xi_2)}{2} \circ (u_h^{n+1} - u_h^n)^2$$
$$\leq F_-'(u_h^n) \circ (u_h^{n+1} - u_h^n).$$

Substituting the above two inequalitties into (3.8), we have that

$$(|\nabla u_h^{n+1}|^2 \nabla u_h^{n+1}, \nabla u_h^{n+1} - \nabla u_h^n) \geq \int_\Omega (F_+(u_h^{n+1}) - F_+(u_h^n)) dx, \tag{3.10}$$

and

$$-(\nabla u_h^n, \nabla(u_h^{n+1} - u_h^n)) \geq \int_\Omega (F_-(u_h^n) - F_-(u_h^{n+1})) dx. \tag{3.11}$$

The identity (3.8) together with (3.9), (3.10) and (3.11) yields that

$$\frac{\epsilon}{2}\|\Delta_h u_h^{n+1}\|^2 + \frac{1}{4}\||\nabla u_h^{n+1}|^2 - 1\|^2$$
$$\leq \frac{\epsilon}{2}\|\Delta_h u_h^n\|^2 + \frac{1}{4}\||\nabla u_h^n|^2 - 1\|^2 - \frac{1}{\Delta t}\|u_h^{n+1} - u_h^n\|_0^2 - \frac{\epsilon\|\Delta_h u_h^{n+1} - \Delta_h u_h^n\|^2}{2}$$
$$\leq \frac{\epsilon}{2}\|\Delta_h u_h^n\|^2 + \frac{1}{4}\||\nabla u_h^n|^2 - 1\|^2,$$

which derives the desired result $E^{n+1} \leq E^n$. □

Theorem 3.2. *The fully discrete scheme* (3.7) *is unconditionally energy-stable.*

Proof. Choosing $v_h = u_h^{n+1} - u_h^n$ in Eq. (3.7), we have

$$\frac{1}{\Delta t}\|u_h^{n+1} - u_h^n\|_0^2 + \frac{\epsilon}{2}\|\Delta_h u_h^{n+1}\|^2 - \frac{\epsilon}{2}\|\Delta_h u_h^n\|^2$$
$$+ \frac{1}{4}(|\nabla u_h^{n+1}|^4 - |\nabla u_h^n|^4, 1) - \frac{1}{2}\|\nabla u_h^{n+1}\|_0^2 + \frac{1}{2}\|\nabla u_h^n\|_0^2 = 0,$$

which implies that

$$
\begin{aligned}
&\frac{\epsilon}{2}\|\Delta_h u_h^{n+1}\|_0^2 + \frac{1}{4}\left((|\nabla u_h^{n+1}|^2 - 1)^2, 1\right) \\
&= \frac{\epsilon}{2}\|\Delta_h u_h^n\|_0^2 + \frac{1}{4}\left((|\nabla u_h^n|^2 - 1)^2, 1\right) - \frac{1}{\Delta t}\|u_h^{n+1} - u_h^n\|_0^2 \\
&\leq \frac{\epsilon}{2}\|\Delta_h u_h^n\|_0^2 + \frac{1}{4}\left((|\nabla u_h^n|^2 - 1)^2, 1\right),
\end{aligned}
$$

namely, $E^{n+1} \leq E^n$. $\hspace{1cm}$ □

Theorem 3.3. *The fully discrete schemes* (3.6) *and* (3.7) *are mass conservative in the discrete sense, i.e.,* $(u_h^{n+1} - u_h^n, 1) = 0.$

Proof. Choosing $v_h \equiv 1$ in (3.6) and (3.7), and applying the properties $\Delta_h v_h = 0$ and $\nabla v_h = 0$, we obtain the desired result. $\hspace{1cm}$ □

3.4 Fully discrete schemes for problem (1.1) with Neumann boundary conditions

In this subsection, we present and discuss two schemes for (1.1) with Neumann boundary conditions by using (3.4), (3.5), and (2.3).

Recalling the bilinear form $a_h(\cdot, \cdot)$ defined in (2.2), we first introduce the discrete bilinear form $a_h(\cdot, \cdot)$ of $a(\cdot, \cdot)$ in the linear finite element space V_h as follows:

$$
\begin{aligned}
a_h(w_h, v_h) = &\int_\Omega \Delta_h w_h \Delta_h v_h dz - \int_{\partial\Omega} \Delta_h w_h (G_h v_h \cdot \mathbf{n}) ds - \int_{\partial\Omega} (G_h w_h \cdot \mathbf{n}) \Delta_h v_h ds \\
&+ \gamma \int_{\partial\Omega} (G_h w_h \cdot \mathbf{n})(G_h v_h \cdot \mathbf{n}) ds, \quad \forall w_h, v_h \in V_h. \hspace{1cm} (3.12)
\end{aligned}
$$

Based on the discrete bilinear form (3.12), we design a fully discrete scheme by combining the formulation (2.3) and the convex splitting method (3.4) for the MBE equation (1.1) as follow:

Scheme 3: The Hessian recovery based linear element scheme with respect to (2.2) reads as: finding $\{u_h^n\}_{n\geq 1} \in V_h$ such that for $n = 0, 1 \cdots, N$,

$$
\begin{aligned}
&\frac{1}{\Delta t}\left(u_h^{n+1}, v_h\right) + \varepsilon a_h(u_h^{n+1}, v_h) + (|\nabla u_h^{n+1}|^2 \nabla u_h^{n+1}, \nabla v_h) \\
&= \frac{1}{\Delta t}(u_h^n, v_h) + (\nabla u_h^n, \nabla v_h), \quad \forall v_h \in V_h, \hspace{1cm} (3.13)
\end{aligned}
$$

where $u_h^0 = \mathcal{P}_h u_0$ and $\mathcal{P}_h$ is the L^2 projection operator on V_h.

The combination of CN approximation and the formulation (2.3) lead to the following fully discretized scheme for (1.1).

Scheme 4: The Hessian recovery based linear element scheme with respect to (2.2) reads as: finding $\{u_h^n\}_{n\geq 1} \in V_h$ such that for $n = 0, 1 \cdots, N$,

$$
\begin{aligned}
&\frac{1}{\Delta t}\left(u_h^{n+1} - u_h^n, v_h\right) + \frac{\epsilon}{2} a_h(u_h^{n+1}, v_h) + \frac{\epsilon}{2} a_h(u_h^n, v_h) \\
&\quad + \left(\frac{|\nabla u_h^{n+1}|^2 + |\nabla u_h^n|^2}{2}\frac{\nabla(u_h^{n+1} + u_h^n)}{2}, \nabla v_h\right) - \left(\nabla \frac{u_h^{n+1} + u_h^n}{2}, \nabla v_h\right) \\
&= 0, \quad \forall v_h \in V_h,
\end{aligned}
\tag{3.14}
$$

where $u_h^0 = \mathcal{P}_h u_0$ and $\mathcal{P}_h$ is the L^2 projection operator on V_h.

Theorem 3.4. *The fully discrete schemes* (3.13) *and* (3.14) *are mass conservative in the discrete sense, i.e.,* $(u_h^{n+1} - u_h^n, 1) = 0$.

Proof. Choosing $v_h \equiv 1$ in (3.13) and (3.14), and applying the properties $\Delta_h v_h = 0$ and $\nabla v_h = 0$, we obtain the desired result. $\square$

Remark 3.3. Our numerical results indicate that Schemes 3 and 4 preserve the energy decay property and have nice convergence properties. Unfortunately, we have not figured out a rigorous proof for the energy decay property of Schemes 3 and 4. The difficulty preventing us from giving a proof similar to Theorems 3.2 and 3.3 resides in the fact that $G_h v_h \cdot \mathbf{n} \neq 0$ for any $v_h \in V_h$, and thus we couldn't bound the last three terms in the formula (3.12).

Remark 3.4. One can also use the penalty method and Lagrange multiplier method to deal with the Neumann boundary conditions. Unfortunately, our numerical results show that both these two methods are unstable.

Remark 3.5. In [17], Guo et al. proposed a gradient recovery based GRBL–FEM to solve biharmonic problems. This GRBL–FEM can be applied to solve the MBE model (1.1). In fact, we can first use the gradient recovery operator to obtain a new discrete Laplace operator $\tilde{\Delta}_r$ as

$$\tilde{\Delta}_r u_h = \partial_x G_h^x u_h + \partial_y G_h^y u_h.$$

Then by utilizing $\tilde{\Delta}_r$ to replace Δ_r in schemes (3.6), (3.13), (3.7) and (3.14), we obtain the GRBL finite element method for MBE model (1.1). Similar to the proofs of Theorems 3.2-3.4, we can also prove that GRBL–FEM method satsifies the properties of energy decay and mass conservation unconditionally. From our numerical experiments, we observe that the GRBL-FEM method also works. However, the GRBL–FEM usually requires a smaller temporal step than the HRBL–FEM.

4 Numerical experiments

In this section, we present several numerical examples to illustrate the robustness and accuracy of the presented numerical schemes. Here we adopt Newton's method to solve

the nonlinear equations at each time step. The tolerance for Newton's method is taken as 10^{-8}.

For convenience, we denote different types of numerical errors by

$$e_0 = \|u - u_h\|_{0,\Omega}, \qquad e_1 = \|\nabla u - \nabla u_h\|_{0,\Omega},$$
$$e_{1,r} = \|\nabla u - G_h u_h\|_{0,\Omega}, \quad e_2 = \|D^2 u - H_h u_h\|_{0,\Omega}, \quad e_\Delta = \|\Delta u - \Delta_h u_h\|_{0,\Omega},$$

and use

$$r = \frac{\log\left(e_h / e_{\frac{h}{2}}\right)}{\log(2)}$$

to demonstrate the convergence orders.

4.1 Test of the accuracy

Example 4.1. In this example, we consider the following MBE problem

$$u_t = -\epsilon \Delta^2 u + \nabla \cdot \left((|\nabla u|^2 - 1) \nabla u \right) + f, \qquad (x,t) \in \Omega \times (0,T), \qquad \text{(4.1a)}$$
$$u(x,0) = u_0(x), \qquad x \in \Omega, \qquad \text{(4.1b)}$$

with $\Omega = [0,2] \times [0,2]$, $T = 1$, $\epsilon = 0.1$. Here the initial solution u_0 and the source term f are chosen such that the exact solution is $u(x,y,t) = 0.1 \exp(-t) \cos(\pi x) \cos(\pi y)$.

In order to test the accuracy in space, we fix the time step size $\Delta t = 10^{-4}$ in (3.6) for periodic boundary condition to compute the numerical solution at $T = 1$, and $\Delta t = 10^{-6}$ in (3.13) for Neumann boundary conditions at $T = 0.01$. Numerical errors with different spacial sizes are depicted in Tables 1-2, respectively. From these two tables, we observe that for both schemes, the L^2-norm errors converge with order 2 while the H^1-seminorm errors converge with order 1 which are both optimal for a linear finite element method. and the recovered H^1-seminorm error is superconvergent of $\mathcal{O}(h^2)$. We also observe that the recovered Laplace and Hessian obtained by (3.6) converge to exact ones with orders 2 and 1.5 respectively, while the convergence orders of both recovered operators obtained by (3.13) are reduced to 1.1. These numerical convergence orders are similar to those obtained in [46] for Cahn-Hilliard equations.

Besides, we also study the performance of the scheme (3.13) on a circular domain $\Omega = \{(x,y) | x^2 + y^2 \leq 1\}$. We choose the exact solution $u(x,y,t) = e^{-t}(x^2 + y^2 - 1)^4$ and f is computed accordingly. Numerical results are demonstrated in Table 3, in which shows that our method using linear elements captures optimal rates of $\mathcal{O}(h^2)$, without any loss of accuracy from the inexact approximation of curved boundaries.

Finally, we also test the convergence rate of the schemes (3.6) and (3.7) with respect to the time discretization in this example. We fix the spacial mesh size $h = 0.01$ and 0.005, respectively. The L^2-norm errors at $T = 1$ with different time steps are shown in Table 5. As expected, the scheme (3.6) gives the accuracy $\mathcal{O}(\Delta t)$ and (3.7) gives the accuracy $\mathcal{O}(\Delta t^2)$.

Table 1: Spatial errors and convergence rates of scheme (3.6) for Test 4.1 with $\Delta t = 10^{-5}$ at $T = 1$.

h	e_0	e_1	$e_{1,r}$	e_2	e_Δ
2/16	4.01×10^{-3}	4.08×10^{-2}	1.42×10^{-2}	7.80×10^{-1}	1.42×10^{-1}
2/32	9.18×10^{-4}	1.72×10^{-2}	3.11×10^{-3}	2.65×10^{-1}	3.21×10^{-2}
2/64	2.32×10^{-4}	8.23×10^{-3}	7.62×10^{-4}	9.18×10^{-2}	7.78×10^{-3}
2/128	5.59×10^{-5}	4.01×10^{-3}	1.91×10^{-4}	3.22×10^{-2}	1.91×10^{-3}
2/256	1.41×10^{-5}	2.01×10^{-3}	4.68×10^{-5}	1.11×10^{-2}	4.92×10^{-4}
r	2.00	1.00	2.00	1.50	2.00

Table 2: Spatial errors and convergence rates of the scheme (3.13) for Test 4.1 with $\Delta t = 10^{-6}$ at $T = 0.01$.

h	e_0	e_1	$e_{1,r}$	e_2	e_Δ
2/16	3.56×10^{-2}	9.56×10^{-1}	1.84×10^{-1}	2.39×10^{-0}	1.60×10^{-0}
2/32	8.54×10^{-3}	4.45×10^{-1}	4.63×10^{-2}	9.89×10^{-1}	6.30×10^{-1}
2/64	2.04×10^{-3}	2.18×10^{-1}	1.15×10^{-2}	4.12×10^{-1}	2.67×10^{-1}
2/128	4.96×10^{-4}	1.08×10^{-1}	2.86×10^{-3}	1.80×10^{-1}	1.22×10^{-1}
2/256	1.21×10^{-4}	5.40×10^{-2}	7.16×10^{-4}	8.25×10^{-2}	5.90×10^{-2}
r	2.00	1.00	2.00	1.10	1.10

Table 3: Spatial errors and convergence rates of scheme (3.13) for Test 4.1 on a circular domain with $\Delta t = 10^{-6}$ at $T = 0.01$.

Dof	e_0	e_1	$e_{1,r}$	e_2	e_Δ
545	5.73×10^{-3}	2.46×10^{-1}	5.21×10^{-2}	1.69×10^{-0}	1.81×10^{-0}
2113	1.66×10^{-3}	1.02×10^{-1}	1.82×10^{-2}	9.09×10^{-1}	9.11×10^{-1}
8231	4.13×10^{-4}	4.66×10^{-2}	5.27×10^{-3}	4.50×10^{-1}	4.56×10^{-1}
33025	1.02×10^{-4}	2.26×10^{-2}	1.47×10^{-3}	2.23×10^{-1}	2.27×10^{-1}
131585	2.52×10^{-5}	1.12×10^{-2}	4.00×10^{-4}	1.11×10^{-1}	1.13×10^{-1}
r	2.00	1.00	1.85	1.00	1.00

Table 4: Spatial errors and convergence rates of scheme (3.7) for Test 4.1 with $\Delta t = 10^{-3}$ at $T = 1$.

h	e_0	e_1	$e_{1,r}$	e_2	e_Δ
2/16	5.48×10^{-3}	3.28×10^{-2}	4.42×10^{-2}	7.80×10^{-1}	1.38×10^{-1}
2/32	1.34×10^{-4}	1.61×10^{-2}	1.11×10^{-2}	2.65×10^{-1}	3.45×10^{-2}
2/64	3.28×10^{-4}	8.03×10^{-3}	2.78×10^{-3}	9.18×10^{-2}	8.34×10^{-3}
2/128	8.36×10^{-5}	4.02×10^{-3}	6.93×10^{-4}	3.22×10^{-2}	2.09×10^{-3}
2/256	2.09×10^{-5}	2.01×10^{-3}	1.73×10^{-4}	1.11×10^{-2}	5.21×10^{-4}
r	2.00	1.00	2.00	1.50	2.00

Table 5: Temporal errors and convergence rate by schemes (3.6) and (3.7) for Test 4.1 at $T = 1$.

Δt	$10^{-1}/2$	$10^{-1}/2^2$	$10^{-1}/2^3$	$10^{-1}/2^4$	r
scheme (3.6)	5.5×10^{-3}	2.7×10^{-3}	1.4×10^{-3}	6.9×10^{-4}	1.0
scheme (3.7)	4.8×10^{-3}	1.1×10^{-3}	2.6×10^{-4}	6.8×10^{-5}	2.0

4.2 Coarsen process

In this subsection, we apply the numerical scheme (3.6) and (3.7) to simulate the MBE equation to show the coarsen process. Since the numerical results computed by the scheme (3.7) are similar to those by (3.6), we only report the numerical results obtained by (4.2). In the following examples, a reasonable time step Δt should be controlled as order $\mathcal{O}(\epsilon)$.

Example 4.2. We consider the following one-dimensional epitaxial growth model suggested in [22,25]:

$$u_t = (u_x^3)_x - u_{xx} - \epsilon u_{xxxx}, \qquad\qquad (x,t) \in [0,12] \times (0,T), \qquad (4.2a)$$

$$u(\cdot,t) \text{ is 12-periodic}, \qquad\qquad\qquad t \in (0,T), \qquad\qquad (4.2b)$$

$$u(x,0) = 0.1\left(\sin\frac{\pi x}{2} + \sin\left(\frac{2\pi x}{3}\right) + \sin(\pi x)\right), \qquad x \in [0,12]. \qquad (4.2c)$$

In this example, we present some numerical results with vary ϵ to show the robustness and accuracy of the proposed algorithm. We set $\Delta t = \epsilon/10$ and the numerical results including height $u_h(x,t)$, gradient $\partial_x u_h(x,t)$ and evolution of the energy are demonstrated in Figs. 1-3.

We set $\epsilon = 0.1$ and $T = 200$, the numerical results obtained by $(h,\Delta t) = (12/128,0.01)$ and $(h,\Delta t) = (12/256,0.005)$ are presented in Fig. 1. Then we set $\epsilon = 0.01$ and $T = 500$ and Fig. 2 gives the results of $(h,\Delta t) = (12/256,0.001)$ and $(h,\Delta t) = (12/512,0.0005)$. Finally, we take $\epsilon = 0.001$ and $T = 1000$ and Fig. 3 presents the results of $(h,\Delta t) = (12/512,0.0001)$ and $(h,\Delta t) = (12/1024,0.00005)$. The little difference between the two lines in Figs. 1-3 indicates that the proposed methods are stable and credible. As we can see from Fig. 1(c), Fig. 2(c) and Fig. 3(c), the energy decays. From Fig. 1(b), Fig. 2(b) and Fig. 3(b), we also observe that the gradient is controlled in the interval $[-1,1]$ and steady states present more waves with a decrease of ϵ, which are in good agreement with [25].

(a)   (b)   (c)
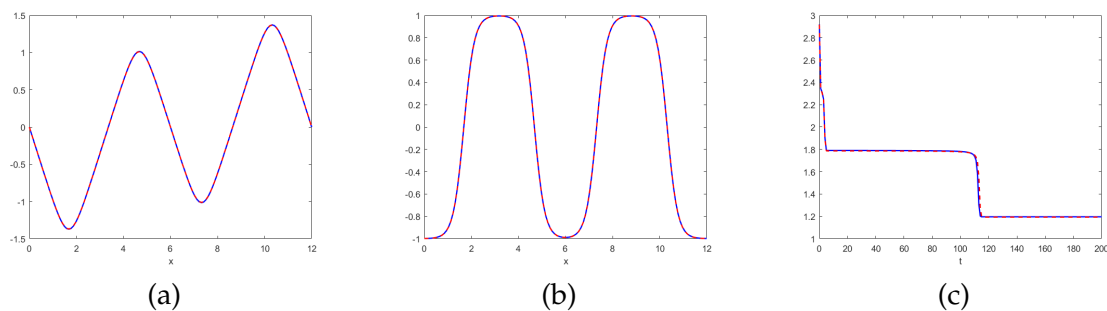
Figure 1: Example 4.2: the results of (a) height: $t = 200$, (b) gradient: $t = 200$ (c) energy: $0 < t < 200$ in the case $\epsilon = 0.1$ obtained with $(h,\Delta t) = (12/128,0.01)$ (solid line) and $(h,\Delta t) = (12/256,0.005)$ (dashed line).
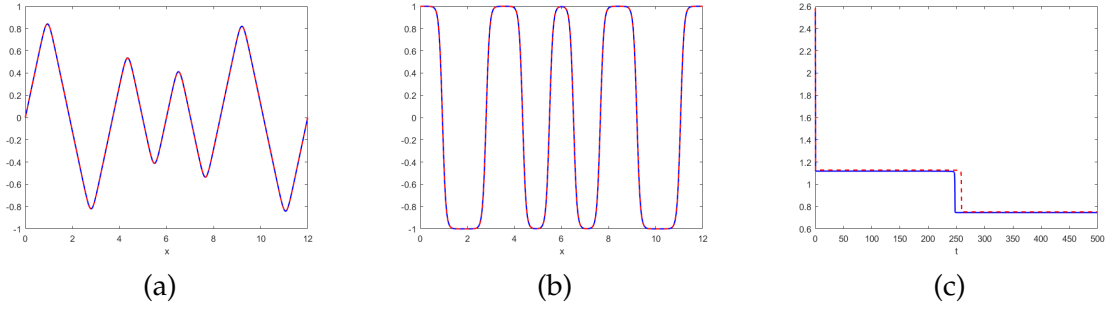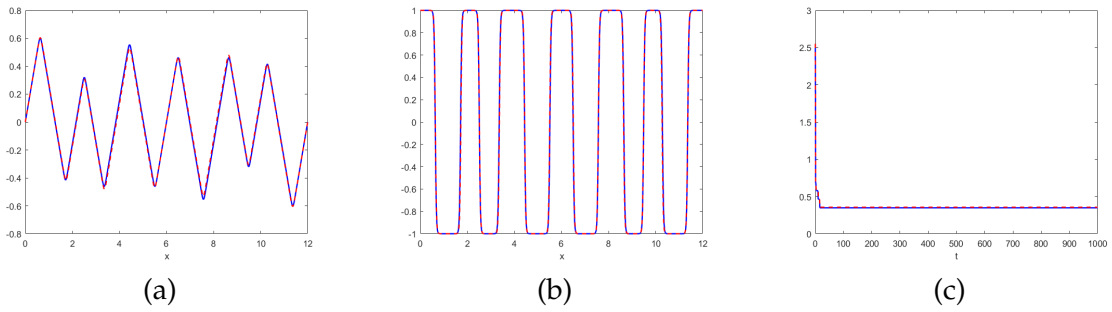
Figure 2: Example 4.2: the results of (a) height: $t=500$, (b) gradient: $t=500$ (c) energy: $0<t<500$ in the case $\epsilon=0.01$ obtained with $(h,\Delta t)=(12/256,0.001)$ (solid line) and $(h,\Delta t)=(12/512,0.0005)$ (dashed line).

Figure 3: Example 4.2: the results of (a) height: $t=1000$, (b) gradient: $t=1000$, (c) energy: $0<t<1000$ in the case $\epsilon=0.001$ obtained with $(h,\Delta t)=(12/512,0.0001)$ (solid line) and $(h,\Delta t)=(12/1024,0.00005)$ (dashed line).

Example 4.3. We consider the two-dimensional MBE model (1.1) with 2π-periodic boundary condition and parameter $\epsilon=0.1$. The initial condition is given by

$$u_0(x,y)=0.1\sin(3x)\sin(2y)+\sin(5x)\sin(5y).$$

This example has been discussed in [22, 32, 35, 47] to study the nonlinear instability of the solution. Here we use the recovered finite linear element method to solve this problem. We set $h=2\pi/100$ and $\Delta t=10^{-3}$, the solution contours obtained by scheme (3.6) at $t=0$, $t=0.05$, $t=2.5$, $t=5.5$, $t=8$, and $t=30$ are plotted in Fig. 4, which agrees well with the published ones presented in [22, 35] by using Galerkin spectral approximations and mixed finite element method.

In this example, we also study the behavior of energy of the MBE growth model. We observe the typical phenomenon in coarsen process. That is, the energy drops quickly at the beginning, then it follows the rough-smooth-rough pattern, finally, it reaches the steady-state. The corresponding numerical results are demonstrated in Fig. 5. In addi-
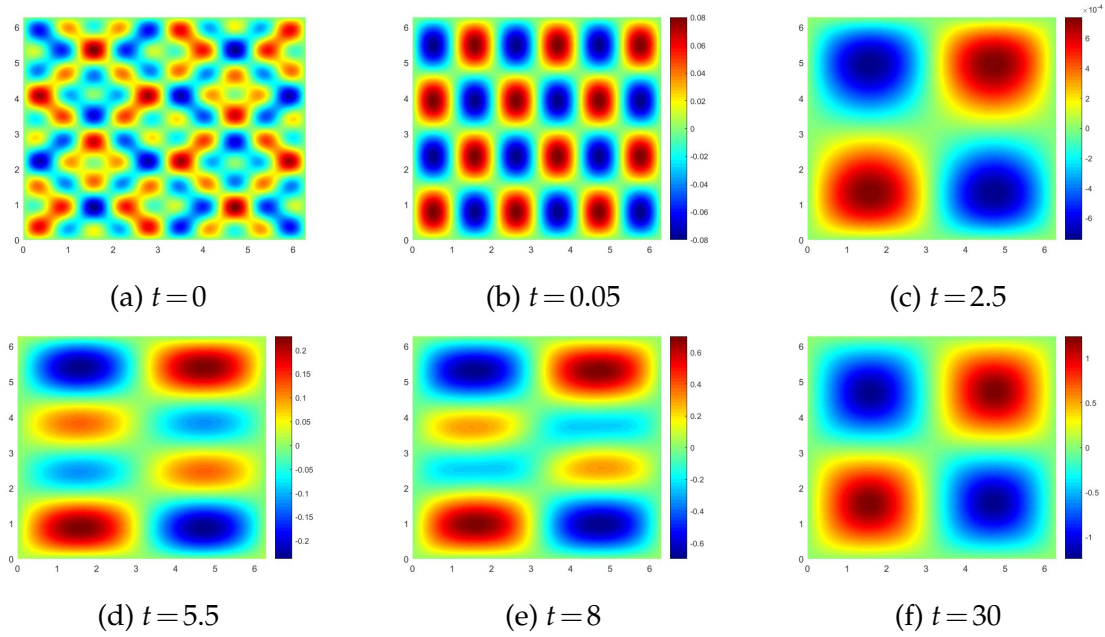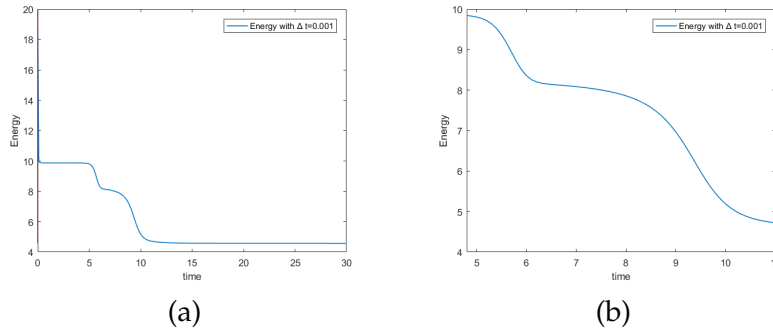
(a) $t=0$ (b) $t=0.05$ (c) $t=2.5$

(d) $t=5.5$ (e) $t=8$ (f) $t=30$

Figure 4: Example 4.3: contour plots of the numerical solutions at $t=0,0.05,2.5,5.5,8,30$.

(a)   (b)

Figure 5: Example 4.3: the evolution of the energy.

tion, we define the roughness of the function u_h^n by

$$R^n := R^n(u_h^n) = \left(\frac{1}{|\Omega|} \int_\Omega (u_h^n - \bar{u}_h^n)^2 dx \right)^{\frac{1}{2}}, \quad \bar{u}_h^n = \frac{1}{|\Omega|} \int_\Omega u_h^n dx.$$

and Fig. 6 gives the evolution of roughness, which is well consistent with the published results in [22, 32, 35, 47].

Example 4.4. We consider the MBE model (1.1) with parameter $\epsilon = 0.1$ on the domain $\Omega = [0,200] \times [0,200]$. The initial data u_0 is a random value by varying from -0.001 to 0.001.

Figure 6: Example 4.3: the development of the roughness.

This example has been studied to verify the power laws for the energy evolution and the height growth during long time evolution in [25, 33]. In this work, the free energy F_{free} and height of the function u_h^n are defined by

$$F_{\text{free}}^n = \frac{1}{4}\left(|\nabla u_h^n|^2 - 1\right)^2 + \frac{\epsilon}{2}|\Delta_h u_h^n|^2,$$

$$H^n = \left(\frac{1}{|\Omega|}\int_\Omega (u_h^n)^2 dx\right)^{\frac{1}{2}}.$$

Since the evolution of rough requires a long time, we choose an adaptive algorithm proposed in [35]. In each step, the time step in scheme (3.6) is updated by the variation of energy. Let $\Delta t^0 = \Delta t_{\min}$, $h = 200/512$ and

$$\Delta t^n = \max\left\{\Delta t_{\min}, \frac{\Delta t_{\max}}{\sqrt{1 + \alpha|(E^n)'|^2}}\right\},$$

where $\alpha = 10^4$, $\Delta t_{\min} = 0.01$, $\Delta t_{\max} = 0.5$ and

$$(E^n)' = \frac{E^n - E^{n-1}}{\Delta t^{n-1}}, \quad n = 1, 2, \cdots, N.$$

The contour lines of the free energy F_{free} at time $t = 2000, 10000, 100000$ are presented in Fig. 7. As expected, the free energy is concentrated on the edges of the pyramidal structures. In Fig. 8, the decay of the energy is observed. In addition, we also present the development of the height. The figures in Fig. 9 are plotted on a log-to-log scale. It is observed that after the early stage of the rearrangement of the structure, the free energy and height nearly satisfy the power law ct^γ with $\gamma = -1/3$ and $\gamma = 1/3$, which matches the existing numerical results.

Example 4.5. In the last example, we consider the two-dimensional MBE model (1.1) with the Neumann boundary condition on a circular domain $\Omega = \{(x,y)|x^2 + y^2 \leq 1\}$, and
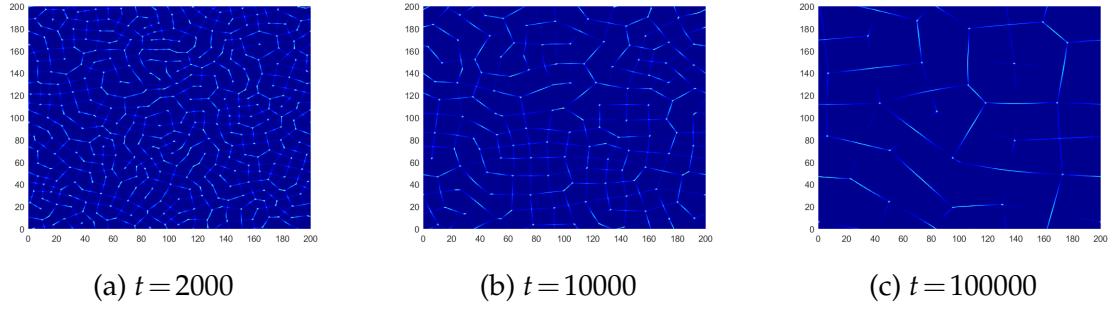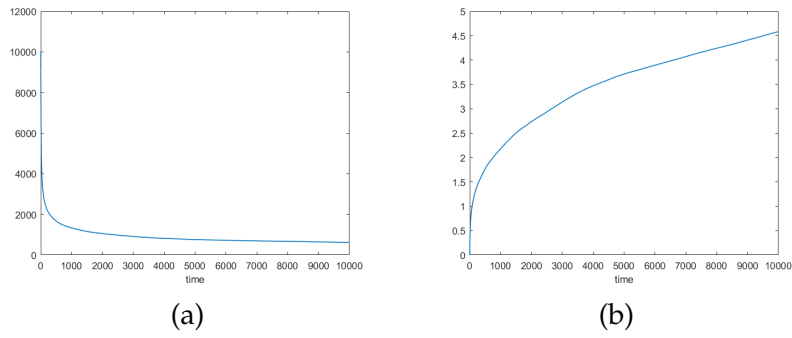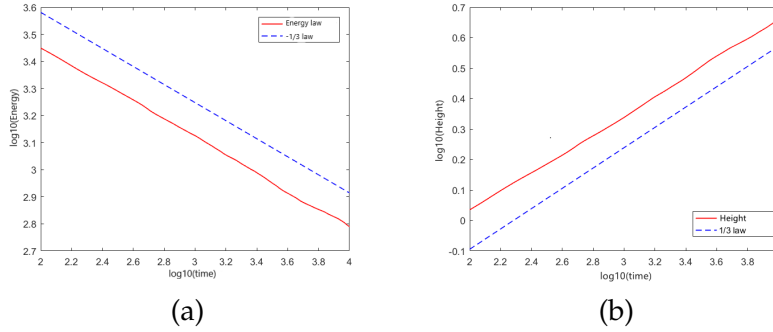
(a) $t=2000$ (b) $t=10000$ (c) $t=100000$

Figure 7: Example 4.4: contour plots of free energy at $t=2000,10000,100000$.

(a)   (b)

Figure 8: Example 4.4: (a): the development of the energy, (b): the development of the height.

(a)   (b)

Figure 9: Example 4.4: (a): $-\frac{1}{3}$-power low for the energy, (b): $\frac{1}{3}$-power low for the height.

parameter ϵ equals to 0.1. The initial condition is given by

$$u_0(x,y)=(x^2+y^2-1)^2.$$

We set $\Delta t=10^{-3}$, the solution contours obtained by the scheme (3.13) at $t=0$, $t=0.1$, $t=0.5$, $t=1$, $t=10$, and $t=30$ are plotted in Fig. 10, and the evolution of the energy is demonstrated in Fig. 11. We observe that the energy also drops very quickly at the be-
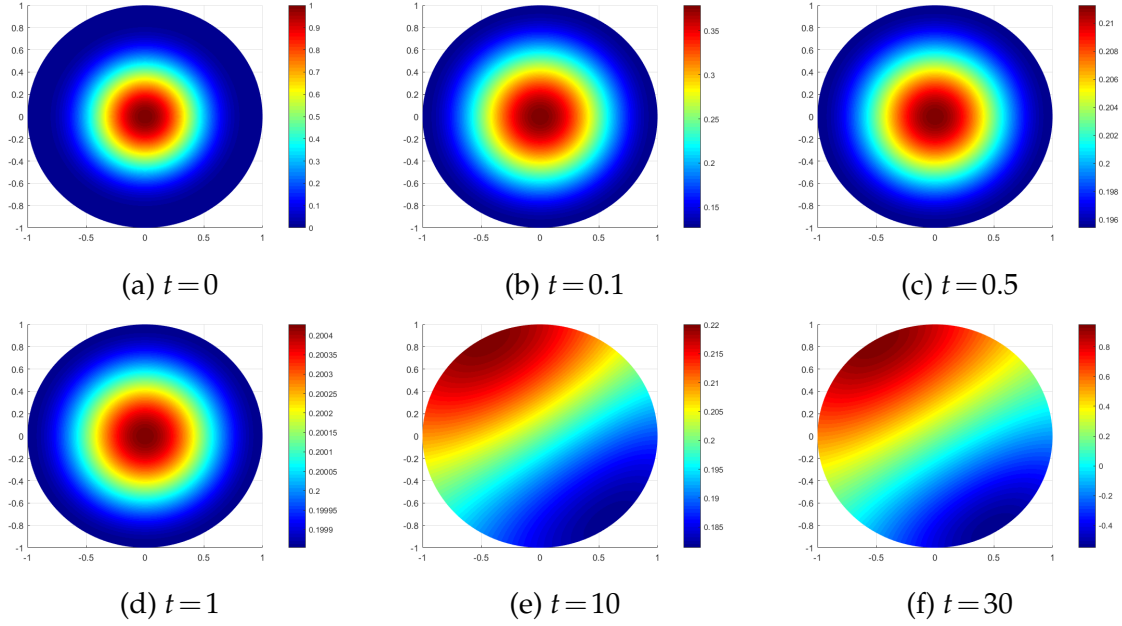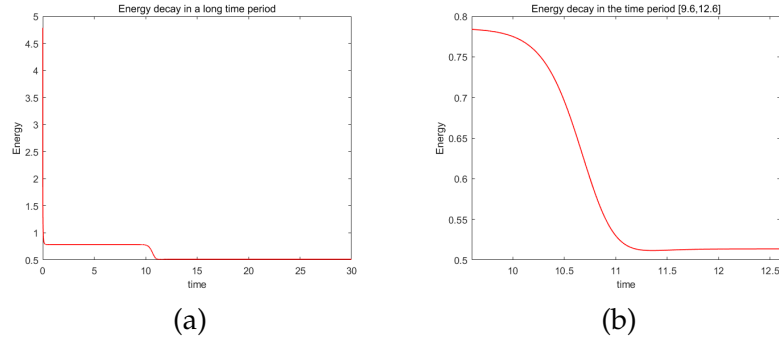
Figure 10: Example 4.5: contour plots of the numerical solutions at $t=0,0.1,0.5,1,10,30$.

Figure 11: Example 4.5: the evolution of the energy.

ginning, then follows a rough-smooth-rough pattern, and finally, reaches a steady state, which is consistent with the typical phenomenon of coarsening.

5 Conclusions

In this work, we apply the Hessian recovery based linear element method to solve the molecular beam epitaxy growth model with slope selection. We prove that the proposed method can capture the physical properties of energy decay and mass conserva-

tion. Meanwhile, numerical results reveal that our presented method is reliable and has the optimal convergence orders. In addition, we also simulate the coarsening dynamics process and observe the 1/3 power law.

It may worth mentioning that the recovered method proposed in this work is more stable and efficient than the gradient recovered method presented in [17] to solve the MBE model. Compared to the Hessian recovery based method in this work, the gradient recovery based method requires a more strict condition on the time step to guarantee the convergence of Newton's iteration. Besides, numerical results indicate that our methods also perform very well for problems on the domain with curved boundaries, without any loss of accuracy from the inexact approximation of curved boundaries. Our methods can be naturally extended to solve time-fractional molecular beam epitaxy models.

Acknowledgements

References

[1] R. ADAMA, Sobolev Space, Academic Press, New York, (1975).

[2] S. CLARKE AND D. VVEDENSKY, *Origin of reflection high-energy electron-diffraction intensity oscillations during molecular-beam epitaxy: a computational modeling approach*, Phys. Rev. Letts., 58 (1987), pp. 2235–2238.

[3] H. CHEN, H. GUO, Z. ZHANG, AND Q. ZOU, *A C^0 linear finite element method for two fourth-order eigenvalue problems*, IMA J. Numer. Anal., 37 (2017), pp. 2120–2138.

[4] W. CHEN AND Y. WANG,*A mixed finite element method for thin film epitaxy*, Numer. Math., 122 (2012), pp. 771–793.

[5] W. CHEN, S. CONDE, C. WANG, X. WANG AND S. WISE, *A linear energy stable scheme for a thin film model without slope selection*, J. Sci. Comput., 52 (2012), pp. 546–562.

[6] R. CAFLISCH, M. GYURE, B. MERRIMAN, S. OSHER, C. RATSCH AND D. VVEDENSKY, *Island dynamics and the level set method for epitaxial growth*, Appl. Math. Lett., 12 (1999), pp. 13–22.

[7] Q. CHENG AND C. WANG, *Error estimate of second order accurate scalar auxiliary variable (SAV) numerical method for the epitaxial thin film equation*, Adv. Appl. Math. Mech., 13 (2021), pp. 1318–1254.

[8] L. CHEN, J. ZHAO AND Y. GONG, *A novel second-order scheme for the molecular beam epitaxy model with slope selection*, Commun. Comput. Phys., 25(4) (2019), pp. 1024–1044.

[9] L. CHEN, J. ZHAO AND X. YANG, *Regularized linear schemes for the molecular beam epitaxy model with slope selection*, Appl. Numer. Math., 128 (2018), pp. 139–156.

[10] L. CHEN, J. ZHANG, J. ZHAO, W. CAO, H. WANG AND J. ZHANG, *An accurate and efficient algorithm for the time-fractional molecular beam epitaxy model with slope selection*, Comput. Phys. Commun., 245 (2019), p. 106842.

[11] G. EHRLICH AND F. HUDDA, *Atomic view of surface diffusion: tungsten on tungsten*, J. Chem. Phys., 44 (1966), pp. 1036–1099.

[12] W. FENG, C. WANG AND S. WISE, *Linearly preconditioned nonlinear conjugate gradeint solvers for the epitaxial thin film equation with slope selection*, arXiv, (2017), pp. 1–15.

[13] W. FENG, C. WANG, S. WISE AND Z. ZHANG, *A second-order energy stable backward differentiation formula method for the epitaxial thin film equation with slope selection*, Numer. Meth. Partial Differential Equations, 34(6) (2018), pp. 1975–2007.

[14] M. GYURE, C. RATSCH, B. MERRIMAN, R. CAFLISCH, S. OSHER, J. ZINCK AND D. VVEDENSKY, *Level-set methods for the simulation of epitaxial phenomena*, Phys. Rev. E, 58 (3) (1998), pp. 6927–6930.

[15] M. GUINA AND S. M. WANG, Molecular Beam Epitaxy, Elsevier, 2013.

[16] H. GUO, Z. ZHANG, AND R. ZHAO, *Hessian recovery for finite element methods*, Math. Comput., 86 (2017), pp. 1671–1692.

[17] H. GUO, Z. ZHANG, AND Q. ZOU, *A C^0 linear finite element method for biharmonic problems*, J. Sci. Comput., 74 (2018), pp. 1397–1422.

[18] B. JI, H. LIAO, Y. GONG AND L. ZHANG, *Adaptive second-order Crank–Nicolson time-stepping schemes for tim-fractional molecular beam epitaxial growth models*, Siam J. Sci. Comput., 42(3) (2020), pp. B738–B760.

[19] H. KANG AND W. WEINBERG, *Dynamic Monte Carlo with a proper energy barrier: surface diffusion and two-dimensional domain ordering*, J. Chem. Phys., 90 (1989), pp. 2824–2830.

[20] R. KOHN AND F. OTTO, *Upper bounds on coarsening rates*, Commun. Math. Phys., 229 (2002), pp. 375–395.

[21] R. V. KOHN AND X. YAN, *Upper bound on the coarsening rate for an epitaxial growth model*, Commun. Pure Appl. Math., 56 (2003), pp. 1549–1564.

[22] B. LI AND J. LIU, *Thin film epitaxy with or without slope selection*, Euro. J. Appl. Math., 14 (2003), pp. 713-743.

[23] B. LI AND J. LIU, *Epitaxial growth without slope selection: energetics, coarsening, and dynamic scaling*, J. Nonlinear Sci., 14 (2004), pp. 429–451.

[24] D. LI, Z. QIAO AND T. TANG, *Characterizing the stabilization size for semi-implicit Fourier spectral method to phase field equations*, SIAM J. Numer. Anal., 54 (2016), pp. 1653–1681.

[25] X. LI, Z. QIAO AND H. ZHANG, *Convergence of a fast explicit operator splitting method for the epitaxial growth model with slop selection*, SIAM J. Numer. Anal., 55 (2017), pp. 265–285.

[26] B. LAMICHHANE, *A finite element method for a biharmonic equation based on gradient recovery operators*, BIT, 54 (2014), pp. 469–484.

[27] L. LU, Q. WANG, Y. SONG AND Y. WANG, *Local structure-preserving algorithms for the molecular beam epitaxy model with slope selection*, Discrete. Cont. Dyn-B., (2020).

[28] F. LUO, H. XIE, M. XIE AND F. XU, *Adaptive time-stepping algorithms for molecular beam epitaxy: Based on energy or roughness*, Appl. Math. Lett., 99 (2020), 105991.

[29] D. MOLDOVAN AND L. GOLUBOVIC, *Interfacial coarsening dynamics in epitaxial growth with slope selection*, Phys. Rev. E, 61 (2000), pp. 6190–6214.

[30] J. NITSCHE, *über ein Variationsprinzip zur Lösung von Dirichlet-Problemen bei Verwendung von Teilräumen, die keinen Randbedingungen unterworfen sind*, Abh. Math. Sem. Univ. Hamburg, 36 (1971), pp. 9–15. Collection of articles dedicated to Lothar Collatz on his sixtieth birthday.

[31] M. ORTIZ, E. REPETTO AND H. SI, *A continuum model of kinetic roughening and coarsening in*

thin films, J. Mech. Phys. Solids, 47(1999), pp. 697–730.

[32] Z. QIAO, T. TANG, AND H. XIE, *Error analysis of a mixed finite element method for the molecular beam epitaxy model*, SIAM J. Numer. Anal., 53 (2015), pp. 184–205.

[33] Z. QIAO, Z. SUN AND Z. ZHANG, *The stability and convergence of two linearized finite difference schemes for the nonlinear epitaxial growth model*, Numer. Methods Partial Differential Equations, 28(6) (2012), pp. 1893–1915.

[34] Z. QIAO, C. WANG, S. WISE AND Z. ZHANG, *Error analysis of a finite difference scheme for the epitaxial thin film model with slope selection with an improved convergence constant*, Int. J. Numer. Anal. Mod., 14 (2017), pp. 1–23.

[35] Z. QIAO, Z. ZHANG AND T. TANG, *An adaptive time-stepping strategy for the molecular beam epitaxy models*, SIAM J. Sci. Comput., 33 (2011), pp. 1395–1414.

[36] L. RATKE AND P. W. VOORHEES, Growth and Coarsening, Springer/Verlag, Berlin, 2002.

[37] J. SHEN, J. XU, AND J. YANG, *A new class of efficient and robust energy stable schemes for gradient flows*, SIAM Rev., 63(1) (2019), pp. 474–506.

[38] J. SHEN AND X. YANG, *Decoupled energy stable schemes for phase field models of two phase complex fluids*, SIAM J. Sci. Comput., 36(1) (2014), pp. 122–145.

[39] J. SHEN, X. YANG AND H. YU, *Energy stable scheme and simulation for multiphase fluids system of naiver boundary condition*, J. Comput. Phys., 284 (2015), pp. 617–630.

[40] J. SHEN AND X. YANG, *Decoupled, energy stable schemes for phase field models of two phase incompressible flows*, SIAM J. Numer. Anal., 53 (2015), pp. 279–296.

[41] J. SHEN, C. WANG, X. WANG AND S. M. WISE, *Second-order convex splitting schemes for gradient flows with Ehrlich-Schwoebel type energy: application to thin film epitaxy*, SIAM J. Numer. Anal., 50(1) (2012), pp. 105–125.

[42] J. VILLAIN, *Continuum models of critical growth from atomic beams with and without desorption*, J. Phys. I, 19(42) (1991), pp. 13–22.

[43] A. WILLOUGHBY AND P. CAPPER, Molecular Beam Epitaxy: Materials and Applications for Electronics and Optoelectronics, Springer, 2019.

[44] C. WANG, X. WANG AND S. M. WISE, *Unconditionally stable schemes for equations of thin film epitaxy*, Discrete Contin. Dyn. Syst., 28(1) (2010), pp. 405–423

[45] Y. XIA, *A fully discrete stable discontinuous Galerkin method for the thin film epitaxy problem without slope selection*, J. Comput. Phys., 280 (2015), pp. 248–260.

[46] M. XU, H. GUO AND Q. ZOU, *Hessian recovery based finite element methods for the two-dimensional Cahn-Hilliard equation*, J. Comput. Phys., 386 (2019), pp. 524–540.

[47] C. XU AND T. TANG, *Stability analysis of large time-stepping methods for epitaxial growth models*, SIAM J. Sci. Comput., 44 (2006), pp. 1759–1779.

[48] X. YANG, J. ZHAO AND Q. WANG, *Numerical approximations for the molecular beam epitaxial growth model based on the invariant energy quadratization method*, J. Comput. Phys., 333 (2017), pp. 104–127.

[49] J. ZHAO, Q. WANG AND X. YANG,*Numerical approximations to a new phase field model for immiscible mixtures of nematic liquid crystals and viscous fluids*, Comput. Methods. Appl. Mech. Eng., 310 (2016), pp. 77–97.

[50] Z. ZHANG AND A. NAGA, *A new finite element gradient recovery method: superconvergence property*, SIAM J. Sci. Comput., 26 (2005), pp. 1192–1213 (electronic).

[51] H. ZHANG, X. YANG, J. ZHANG, *Stabilized invariant energy quadratization (S-IEQ) method for the molecular epitaxial model without slope section*, Int. J. Numer. Anal. Mod., 18(2021), pp. 642–655.

[52] O. ZIENKIEWICZ, R. TAYLOR, AND J. ZHU, The Finite Element Method: Its Basis and Fun-

damentals, Elsevier/Butterworth Heinemann, Amsterdam, Seventh ed., 2013.

[53] O. ZIENKIEWICZ AND J. ZHU, *The superconvergent patch recovery and a posteriori error estimates. I. The recovery technique*, Int. J. Numer. Methods Eng., 33 (1992), pp. 1331–1364.